university of groningen / faculty of science and engineering

# Energetic tin ions traversing a hydrogen gas: Electron exchange reactions

University of Groningen

Bachelor Research Project

Applied Physics

*Author:*
Thomas Veringa Weiler S2978024
*Daily supervisor*
S. Rai

*First examinor*
Prof. dr. ir. R. Hoekstra
*Second examinor*
Dr. T.A. Schlathölter

Februari 3, 2020

# Abstract

EUV light, made by a laser produced plasma of tin ions, provides the next step in the chip manufacturing process. To ensure a long lifetime for the collector mirror situated inside the laser, hydrogen gas is used as a stopping gas for the high energy tin ions inside the laser chamber. This thesis provides a first look into the reaction products from the charge exchange between high energy tin ions and hydrogen gas molecules. Additionally, it presents insight into how the setup can be improved upon to acquire more accurate results.

# Contents

# 1 Introduction

In a society that is ever increasingly dependent on technology, the development of smaller sized microchips is (and will for the foreseeable future be) a booming business. If you can manufacture a smaller chip, you can make your electronic devices smaller or you can fit more chips into the same volume. So it is no surprise that chip manufacturers such as Intel and Samsung are pushing the limits when it comes to the fabrication of smaller and smaller chips. To give you an idea of how small chips are getting these days, in 2017, Intel had already managed to fabricate chips with over a hundred million transistors per square millimeter [1].

Of course not only the chip manufacturers are competing to make the smallest and most efficient chips. Also the companies making the chip fabrication machines invest heavily into the research on making machines that further reduce microchip size. Chips are made using a process called optical nano-lithography or photo-lithography, in which concentrated beams of photons with short wavelength and thus high energy produce a pattern onto a semi-conductor wafer. The circuit itself is then etched onto the pattern to produce the chip. In this process it is important to note that the dimensions of the microchip features and thus its transistor density increases with decreased photon wavelength.

ASML is the current leader on the supply of photo-lithography systems, since it is the first and currently only company to not only produce deep ultraviolet (or DUV) lithography machines, but also supply extreme ultraviolet (or EUV) lithography machines [2]. Keeping in mind that EUV light has a wavelength that is 14 times as small as DUV light (EUV light has a wavelength of $13.5nm$ compared to the wavelength of DUV light, $193nm$), one can understand why EUV lithography machines enable higher density chip manufacturing.

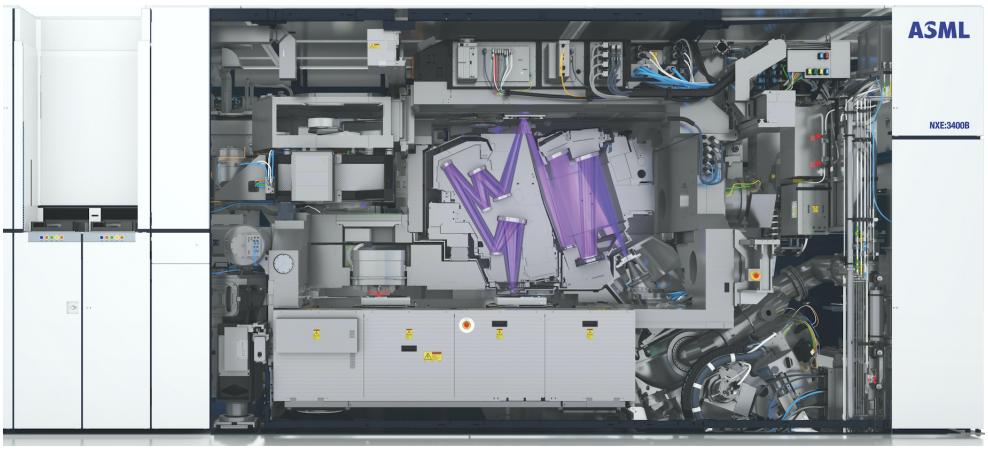


**Figure 1.1:** An EUV lithography machine as seen from the inside. *Image adapted from [3].*

This EUV light is produced by a laser produced plasma (or LPP for short) of charged tin ions [4]. By shooting a laser at a tin droplet target, the droplet explodes into a plasma of tin ions, producing the desired EUV light. A hemispherical collector mirror is placed around this plasma to focus the EUV light toward the lithography machine. A challenge in the production of the EUV light is the fact that highly energetic tin ions can damage the mirror and thus the laser effectiveness. To prevent this, hydrogen gas is injected through the vacuum chamber containing the LPP and collector mirror, in order to absorb the impact of flown high energy tin ions. However not much is known about the interaction between tin ions and hydrogen molecules, so this research focuses on the electron exchange reactions between energetic tin ions and a hydrogen gas.

# 2 Theory

In this section, the theory behind the experiments done will be explained briefly. Most importantly, the process under which charge exchange takes place will be described. In addition, the origin of the reaction products will be made clear. Lastly, the theory behind the ratio of reaction products measured will be explained.

## 2.1 The overbarrier model

Electronic processes between ions and molecules can happen in many ways. However, in $keV$ ion-atom collisions, electron capture is the predominant reaction [5]. Electron capture occurs according to the reaction

$$A^{q+} + B \longrightarrow A^{(q-n)+} + B^{n+}, \tag{1}$$

In which $A$ represents the ion and $B$ the target atom or molecule.

An instructive way to describe the electron capture that takes place, is through the overbarrier model [6]. In figure 2.1 you can see an ion $A^{q+}$ (represented by the yellow dot) and a molecule $B$ (represented by the blue and white dot) approach each other. Their respective electrons (red dots) lie in the molecule's potential well. As they come near to each other, the potential barrier in between them decreases and at short distance a joint potential energy well for the electrons is formed. If the barrier comes below the ionization energy of a particular electron, the electron can move over toward the ion. Eventually the ion and target molecule move away from each other, keeping the electron trapped in the ion's potential well.

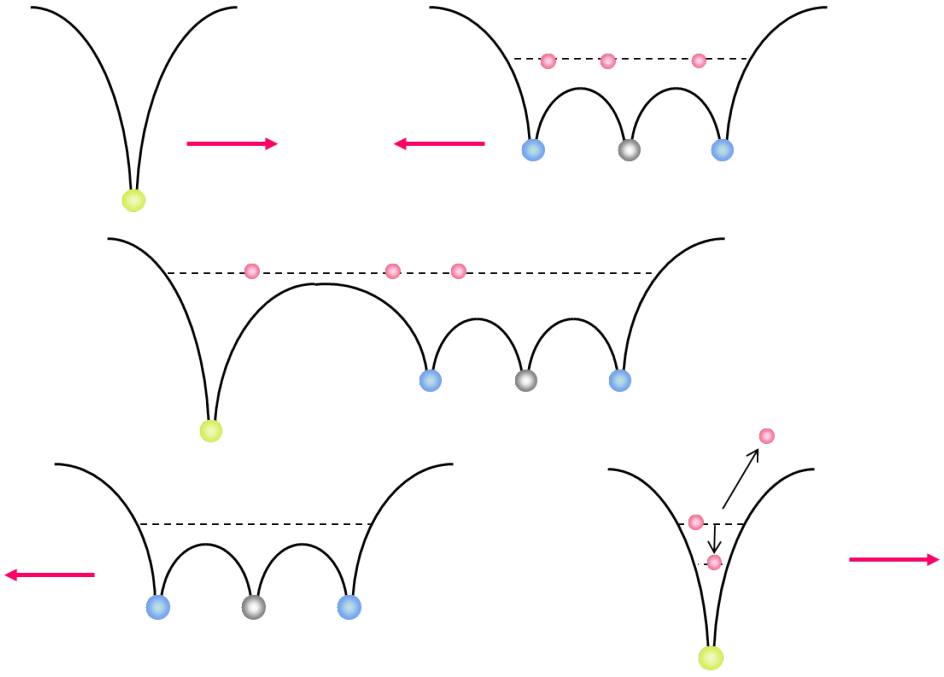

**Figure 2.1:** A visual representation of the overbarrier model. *Image adapted from [7].*

Because the molecule has lost electrons, the ion and molecule now both have positive charge and thus repel off each other, so the molecule may gain some kinetic energy. However, this gained kinetic energy is typically much less than 1 $eV$ [8]. So in case of a dissociation of the target molecule, the associated

kinetic energy release dominates over the recoil energy. This dissociation will be explained thoroughly in the following section.

## 2.2 Molecular hydrogen energy levels

The target hydrogen's fate largely depends on its internal energy after the charge exchange reaction. The first thing to note is the fact that the charge exchange time between the ion and hydrogen is much shorter than the dissociation time of the molecule. Thus we can assume that during the charge exchange (and thus the excitation of the hydrogen molecule) the internuclear distance between the hydrogen atoms remains fixed. In other words, the electronic transitions follow the Franck-Condon principle. The effect of that can be explained with the help of the figure below.

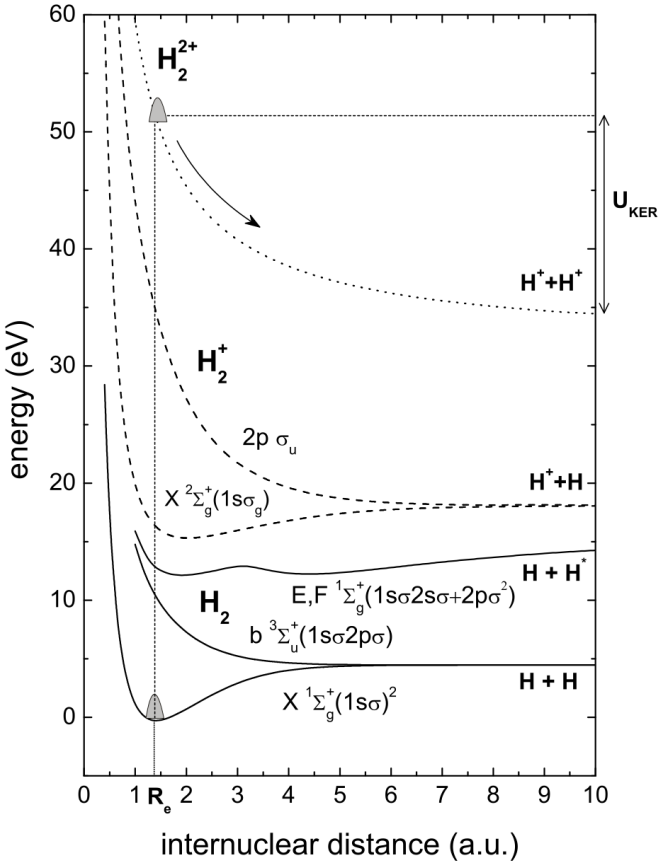


**Figure 2.2:** Potential energy curves for molecular hydrogen and its most important ionized excited states. *Image adapted from [9]*

Consider a hydrogen molecule in rest. As the reaction occurs, the ionized molecule is excited and thus gains potential energy (as seen in figure 2.2). Since the internuclear distance remains the same during the electron capture by the ion, this corresponds to a vertical transition in the diagram. Depending on the amount of energy the hydrogen has gained and electrons it has lost, its transition stops at either of the dashed lines or the dotted line. From this point on several things can happen, which will be discussed in detail below.

To take a look at the first reaction that can occur, consider the reaction where the hydrogen molecule loses 2 electrons and thus becomes $H_2^{2+}$. The transition then ends on the dotted line in the diagram. Since this state is not stable, the internuclear distance of the hydrogen molecule increases and follows the

arrow on the diagram. This continues until the molecule has completely dissociated into two protons. This loss of potential energy results in a gain of kinetic energy for both protons. In the diagram the kinetic energy release is denoted by $U_{KER}$ and has a value of approximately 16 $eV$. The energy is split evenly between the two protons, so that both gain a kinetic energy of 8 $eV$. From now on we'll refer to this reaction as 'reaction 1'.

If the hydrogen molecule only loses one single electron, two things can happen, depending on the amount of energy gained. If the hydrogen ion gains about 35 eV, the $H_2^+$ ion ends up in the $2p\sigma_u$ level, or the upper dashed line. Similarly to the option described before, this state is not stable and the two nuclei dissociate into a proton and a hydrogen atom. The potential energy loss, and thus gain in kinetic energy, of about 17 $eV$ is again split evenly between the two fragments. We'll refer to this reaction as 'reaction 2'.

If the hydrogen ion gains between 16 and 20 eV, the transition lands on the lowest dashed line. From here on the molecule can do either of two things. Firstly, the nuclei dissociate into a hydrogen atom and a proton. However in this process, they barely gain any kinetic energy. We will call this 'reaction 3' from now on. The $H_2^+$ ion however doesn't necessarily have to dissociate, but can also survive as a $H_2^+$ molecule, again barely gaining any kinetic energy. We will refer to this as 'reaction 4'.

## 2.3 Detection of the reaction products

The direction in which the protons (and $H_2^+$ molecules) gain their kinetic energy is random. As will be explained in more detail in section 3, the produced ions in the reaction chamber are extracted towards the micro-channel plate detector by an electric field. However, in between the reaction chamber and the tube towards the detection device, a diaphragm is placed. Not all reaction products can pass through this diaphragm. Therefore, in comparing the different reaction occurrences, a correction has to be made regarding their respective transmissions through the diaphragm.

To paint a picture of why transmissions for the different reaction products can be different, imagine an $H_2$ molecule dissociating into two protons in between two plates. A voltage is put over the two plates, so as to push both in the direction of the plate with a hole in it. It is important to note that the kinetic energy both protons receive is equal but opposite in direction. A representation of what this could look like can be found in figure 2.3. From the figure, you can clearly see how the proton that starts with a velocity to the right makes it through the diaphragm and can be detected. The other proton hits the extraction plate and can thus not be detected. The implications of this are discussed in section 4.1.

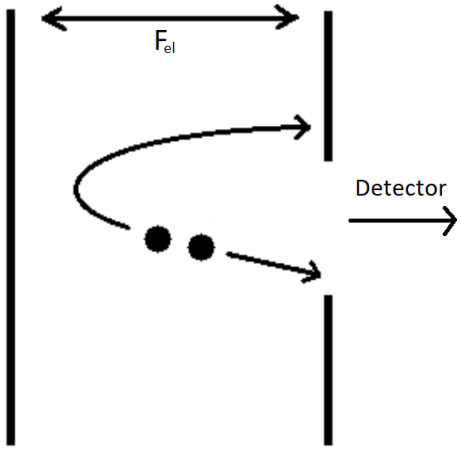


**Figure 2.3:** Schematic representation of a dissociation of $H_2^{2+}$ into two protons, under the influence of an electric field.

# 3 Experimental setup

In this section the different components of the setup for the experiment are outlined and explained in detail. An overview of the setup can be seen in figure 3.1.

The atoms are ionized inside a supernanogan type ECRIS. After being extracted out by a puller lens, the beam of ions is bent and filtered as per the $\frac{m}{q}$ ratio by a 110° bending magnet. The beam is then focused using a quadrupole triplet and doublet, after which it enters the reaction chamber CHEOPS. The different ions created there are extracted under an electric field, focused again by a number of lenses and detected by a microchannel plate detector, which sends the signal towards the computer.

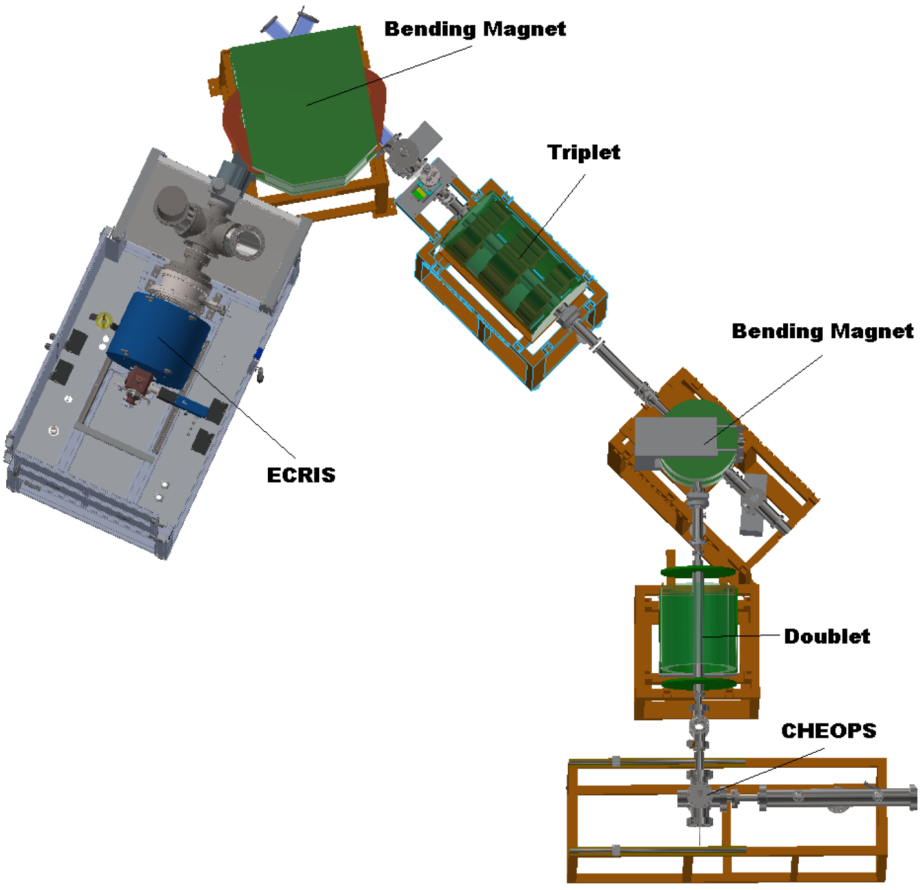


**Figure 3.1:** Top-down 3-dimensional view of the setup. The ion beam is transported from the ECRIS towards the collision chamber called CHEOPS. *Image adapted from [10].*

## 3.1 ECRIS

The ECRIS, which stands for Electron Cyclotron Resonance Ion Source, is as the name suggests the source of the ions that are transported towards the reaction chamber. The ECRIS consists of a number of parts, as can be seen in figure 3.2.

The plasma chamber in the middle is surrounded by a cylindrical permanent magnet, under which influence the electrons in the chamber start gyrating. When microwave photons are radiated into the chamber (labelled by 'RF 14 GHz' in figure 3.2) the electrons are accelerated if their gyration frequency

resonates with that of the RF source. These highly energetic electrons can then ionize atoms and ions present in the plasma chamber. Both gases and tin evaporated by an oven can be injected into the chamber. The gas inlet can also be seen in figure 3.2. The tin oven is located inside the chamber. In this oven, a filament encases a rod of tin. By applying a voltage on the filament, the tin melts and can then evaporate inside the plasma. The ions can be extracted by applying a voltage on the source (with a maximum voltage of 25 kV). The energy the ions obtain upon extraction can be calculated by

$$E_k = qV. \tag{2}$$

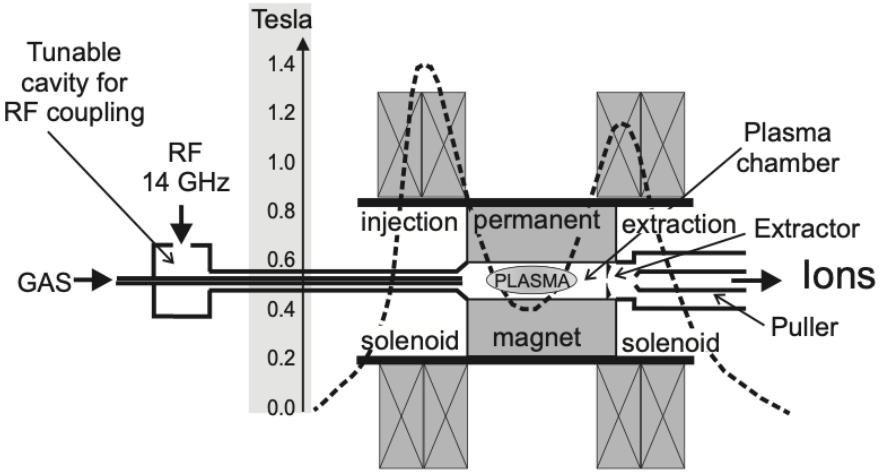


**Figure 3.2:** Old schematic overview of the different parts of the ECRIS. The solenoids and magnetic field plot are to be ignored, since the values are no longer true. *Image adapted from [9].*

## 3.2 Ion beam transportation

### 3.2.1 Einzel lens

Located directly after the puller lens is a couple of focusing lenses serving the purpose of an Einzel lens. An Einzel lens consists of 3 cylindrical electrodes in a row, each of which can have a different potential (as seen in figure 3.3).

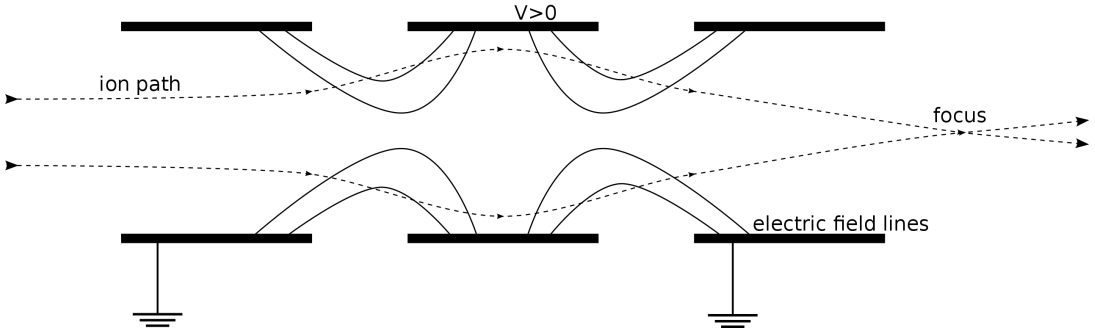


**Figure 3.3:** Schematic overview of an Einzel lens. *Image adapted from [11].*

Often (as is also the case in this particular setup) the potentials of the first and third electrode are set to zero. The second electrode is set to a positive potential. Because of the positive potential difference between the first and second electrode, the ion beam starts to diverge. Between the second and third

electrode, of course, the reverse happens and the ion beam converges. The focal point can be altered by adjusting the positive voltage set on the second electrode. The Einzel lens was used sparsely throughout the experiments.

### 3.2.2 Bending magnet

Situated about a meter after the Einzel lens is the first bending magnet. As the name suggests, it bends the beam over an angle of 110° with the use of a magnetic field. It consists of two large horizontally placed copper coils situated above each other with the ion beam passing in between the coils. Based on the magnitude of the current applied to the coils, a magnetic field B is generated applying a Lorentz force ($F_L$) on the ions

$$F_L = qvB, \tag{3}$$

Where q represents the ion charge and v the velocity of the ions. To find out over which bending radius the ions are bent, we need to equate the formula for the Lorentz force to the formula for the centripetal force

$$F_{centr} = \frac{mv^2}{r}. \tag{4}$$

By recombining the formulae you can obtain a formula for r:

$$r = \frac{mv}{qB}. \tag{5}$$

the velocity can be obtained by equating the formula for the kinetic energy to the formula for the energy of a charged particle

$$\frac{mv^2}{2} = qV, \tag{6}$$

from which we can derive

$$v = \sqrt{\frac{2qV}{m}}. \tag{7}$$

By plugging equation 7 into equation 5 and recombining, we obtain a formula for the magnetic field under which the ions bend

$$B = \sqrt{\frac{m}{q}} \cdot \frac{\sqrt{2V}}{r}. \tag{8}$$

As you can see from this equation, the magnetic field needed to bend the ions over a circle angle with radius r depends on their mass-to-charge ratio $\frac{m}{q}$. Any ions that do not have the correct mass-to-charge ratio are not bent under the right angle and thus scatter away from the desired ion beam path. This is very useful, since this means you can set the bending magnet's magnetic field to a desired magnitude for which only ions with the desired mass-to-charge ratio can propagate further down the ion beam path. So the bending magnet is very useful for filtering out all ions that are not to be measured.

As can be seen in figure 3.1 there is another bending magnet, one which bends the ion beam 45°. This bending magnet works in the same way as was explained about the 110° bending magnet.

### 3.2.3 Beam focusing quadrupole magnets

In between the two bending magnets is a quadrupole magnet triplet. This triplet is there to refocus the ion beam. Just as the bending magnets it uses the Lorenz force to bend the ion trajectories, albeit for another purpose. A schematic drawing of how the quadrupole works can be seen below.

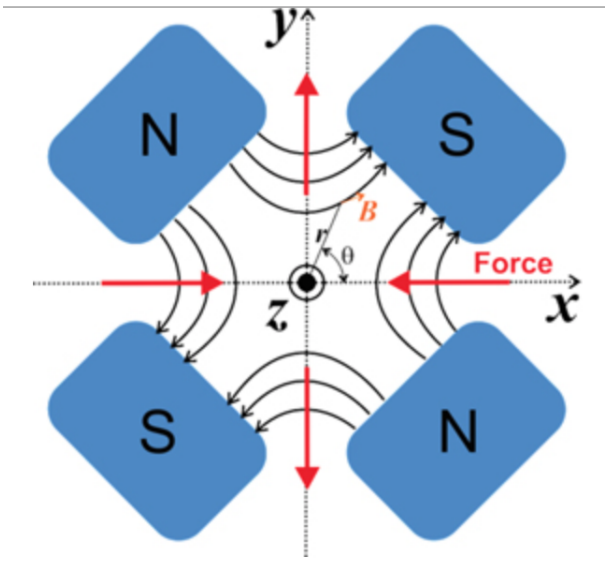


**Figure 3.4:** Schematic overview of the forces involved in a quadrupole. Notice how because of the positioning of the different poles, the beam width is elongated in one direction and pressed in the other. *Image adapted from [12].*

Because the North poles are situated across each other with two South poles in between, the ion beam is stretched in the positive and negative y-axis direction and pressed in the positive and negative x-axis direction. This would make for an ovally shaped beam. However there is another quadrupole placed behind the first one, rotated 90° with respect to the first quadrupole in the plane of incidence. Behind that one there is a third quadrupole, also rotated 90°, hence the name triplet. The three quadrupoles together help to focus the ion beam. Each of the quadrupoles' magnetic field can be changed, to allow for better beam focusing.

Between the 45° bending magnet and CHEOPS is a quadrupole doublet. As the name suggests, it consists of two quadrupoles instead of 3, again rotated by 90° with respect to each other.

### 3.2.4 CHEOPS

The reaction chamber where the ion beam meets the hydrogen gas is called CHEOPS, which is short for CHarge Exchange Observed by Particle Spectroscopy. On top of the chamber, a flow controller is placed which controls the amount of hydrogen gas that is let into CHEOPS. The hydrogen gas flows through the flow controller and exits through a needle located in the center of the reaction chamber, right above where the ion beam crosses CHEOPS. Inside the reaction chamber, two extraction plates ensure that the products of the charge exchange reactions exit CHEOPS, which will be explained in the subsection labeled 'Extraction'.

## 3.3 Signal detection and processing

### 3.3.1 Faraday cup

To measure the ion beam current that is extracted from the source and flows through the setup (specifically at CHEOPS), two Faraday cups are placed. One is located between the 110° magnet and the quadrupole triplet, the other on the end of CHEOPS. A schematic drawing of a generic Faraday cup can be seen in figure 3.5.

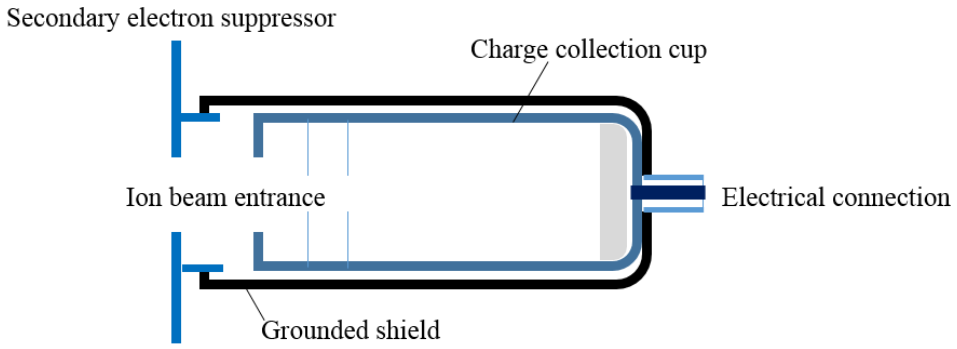


**Figure 3.5:** Schematic drawing of a Faraday cup, with all its components labelled accordingly. *Image adapted from [13].*

Ions enter the Faraday cup through the ion beam entrance. Upon making contact with the charge collection cup, the ions are neutralized, causing the cup to charge up. When the cup is discharged and is connected to a circuit, a small current starts to flow. This can in turn be measured by a current measuring device. The secondary electron suppressor is put on a voltage to prevent secondary electrons (which are ejected by the ions hitting the charge collection cup) from leaving the Faraday cup and negatively influencing the measured charge accuracy.

### 3.3.2 Time of Flight

In order to measure in what quantities what reactions take place inside CHEOPS, the Time of Flight method is used. Its basic principle is quite simple. Start a clock every time a reaction starts and measure the time it takes for the reaction products to reach the detector. In the setup used in this experiment, that happens in the following way (keep in mind that all parts mentioned below will be explained in detail in the next sections).

First, the continuous ion beam is pulsed by a chopper system. Every time an ion beam is pulsed, the clock is started. Inside CHEOPS, the reaction products are extracted in the ToF spectrometer by applying a voltage to the two extraction plates. The reaction products are then focused again by a lens system and hit the detection device, a micro-channel plate detector, to generate a stop signal. The difference in time between the ion beam passing the chopper-sweeper system and a reaction product hitting the micro-channel plate detector is measured and noted down by the computer. After a chosen amount of time, all counts are collected and a graph can be made which shows the number of times a reaction product has hit the detector per timescale.

### 3.3.3 Chopper system

As previously mentioned, the chopper system chops the continuous ion beam into small bunches. Every time a bunch of ions passes the chopper system, the clock of the Time of Flight system is started. The

chopper system consists of two plates placed on top of each other with the beam crossing through the center. When a positive voltage is applied to one of the plates and a negative voltage is applied to the other, the beam is bent so that it can no longer pass through the system but hits the wall. If after some time the applied voltages are reversed, the beam is bent in the exact opposite direction. While the beam bends from the one wall towards the other, there is a small portion of time in which the beam is directed straight out of the diaphragm behind the chopper plates. This creates an ion beam pulse of a few tens of nanoseconds wide. The switching of plate voltage is done with a frequency between 1 $kHz$ and 8 $kHz$.

### 3.3.4 Extraction

Once the projectile ions and hydrogen molecules have exchanged electrons, the reaction products must be extracted so that they can be detected by the micro-channel plate detector. To do this, two metal extraction plates are located on both sides of the ion beam, right where the ions interacts with the hydrogen gas. One of the plates is a solid disc on which a positive voltage is put. The other disc has a 5 $mm$ diaphragm in its center, and is exposed to a negative voltage. Because of this potential difference, the positively charged reaction products are pushed away from the first disc and pulled into the hole of the second disc. The projectile ion beam energy is so high, it will only slightly change direction due to the electric field.

Behind this diaphragm is a set of cylindrical electrodes, which work in the same way to those in the Einzel lens. They also serve the same purpose of focusing the reaction products. In addition to focusing the ion trajectories, they also accelerate the ions.

Located after the 3 focusing electrodes is the Time of Flight (TOF) tube. This tube is wider and much longer than the focusing electrodes. A negative voltage is put on the TOF tube so the ions are further sped up towards the micro-channel plate detector.

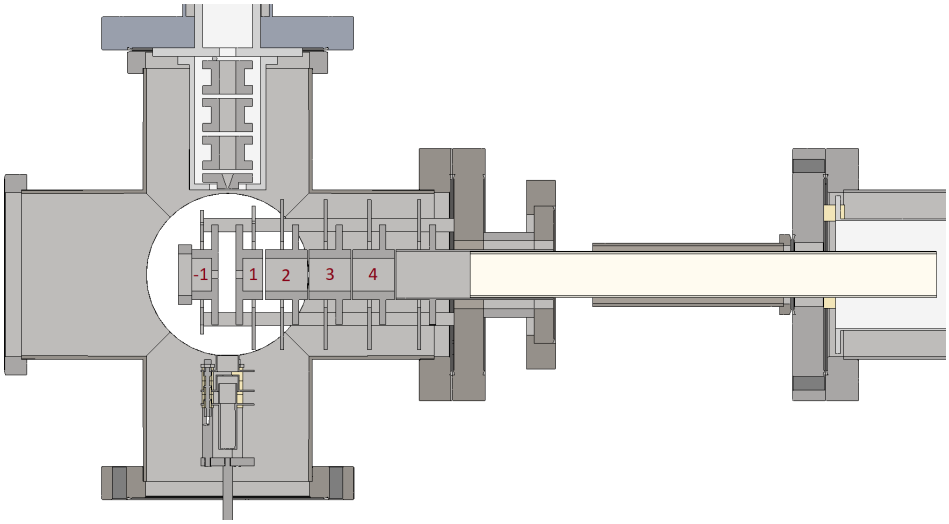


**Figure 3.6:** Schematic of the inside of CHEOPS and the extraction tube. The extraction plates are marked -1 and 1. The focusing lenses are marked 2, 3 and 4.

### 3.3.5 Micro-channel plate detector

To accurately detect each ion created in the charge exchange, a Faraday cup is not sensitive enough. Therefore a micro-channel plate detector is used. It is a small disc filled with holes with a diameter of about $10\mu m$ [14]. When an ion hits a channel wall, the wall emits secondary electrons resulting in a cascade of electrons. A voltage is applied on the MCP, so that the electric field caused by it ensures that the electrons are accelerated toward the back of the channel. The back of the MCP is connected to an anode, upon which the shower of electrons are collected. The anode then passes the signal through. To prevent any ions passing through a channel without hitting the wall, all channels are set at an angle between 5° and 15° with respect to the vertical axis to plate surface.

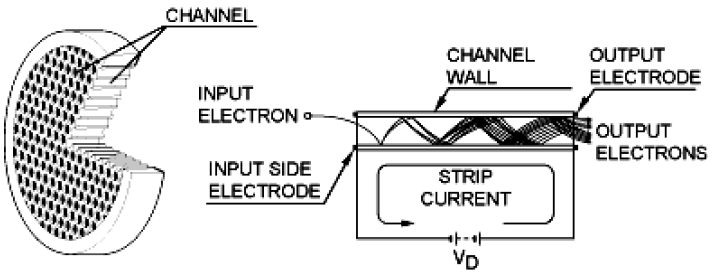


**Figure 3.7:** Cutaway view and schematic view of a single channel. Notice how a single hit produces a shower of electrons on the end of the channel. *Image adapted from [14].*

# 4 Results and discussion

Prior to the experiments listed below, many test and calibration experiments were done with Helium and Hydrogen ions directed at a hydrogen gas. The experiments below are a follow-up on these experiments.

## 4.1 Measurements with $Sn^{5+}$ as projectile ions

Most importantly, the first measurements with a tin ion beam were done. This is an important step, since the goal of all experiments together is to eventually be able to determine charge exchange cross sections of tin ions with different charge and energy. However before measurements were started, some choices had to be made regarding the tin ions.

First, the tin isotope used had to be chosen. Tin has ten naturally occurring stable isotopes. For the experiment it is nice to have a high current ion beam, since that means more ions are present in the beam and thus more charge exchange reactions occur in a given time period. This means that a measurement can be done more quickly. The logical choice was therefore to use the tin isotope with the highest abundance, which is $^{120}Sn$ (with an abundance of around 33%).

The next thing that had to be chosen was the charge state of the tin. For this choice it is very important to note that atoms or molecules with the same mass-to-charge ratio $\frac{m}{q}$ move in the same path in vacuum and are identically affected by magnetic fields. So to make sure that the ion beam isn't contaminated with ions with similar mass-to-charge ratio, you have to choose a correct mass-to-charge ratio. In this case a charge state of 5+ was chosen, since there is a very small chance that there would be a molecule present in the ion source plasma with $\frac{m}{q} = 24$.

Once a beam was made with the right energy and mass-to-charge ratio, we had to make sure that the beam was actually tin and not some other element or molecule. To do that, the magnetic field of the 110° magnet was first raised and then lowered gradually. Every isotope of tin has a different mass and natural abundance. The ratio of abundance between $^{120}Sn$ and any other isotope should be the same as the ratio of the respective ion currents measured. So by for example gradually decreasing, the tin isotopes $^{119}Sn$, $^{118}Sn$, $^{117}Sn$ and so forth could be found by monitoring the beam current. If the abundance and current ratios would be similar, it would surely have to be a tin beam.

After all the mentioned parameters were set, the measurements were started. The outcome of these measurements can be found in figure 4.1. In the spectra, the different reactions as mentioned in section 2.2 can be found. We can now link the different reactions to the peaks as found in figure 4.1. The first and third peak from the left, so peak 1 and 3, correspond to the reactions where fast moving ions are created. They can thus be linked to reactions 1 and 2 of section 2.2. Peak 2 represents the creation of near zero-energy protons, so reaction 3 of the theory. The large peak on the right, peak 4, corresponds to the creation of near zero-energy $H_2^+$ ions, so reaction 4.

The first thing that stands out, is the very large difference in peak height between the first three (proton) peaks and the fourth ($H_2^+$) peak. This tells us that the reaction in which $H_2^+$ is made has a significantly larger cross section than those of the other reactions. The best peak to compare peak 4 with is peak 2, since both corresponding reactions come from the same type of charge exchange reaction. The ratios between peak 4 and 2 can be found in table 1. For 60 $keV$ and 90 $keV$, the ratios seem similar, however for 120 $keV$, the ratio jumps up. More measurements should be done to test the validity of this conclusion. Also it is currently not known why this is the case. In any case it can be said that excited $H_2^+$ molecules have a very low chance of dissociating into a proton and hydrogen atom.

The second thing that can be clearly seen from the graphs is the fact that peak 1 is always larger than peak 3. This is due to the transmission difference, as explained in section 2.3. However, not much can be said on the ratio between the two, since that is highly dependent on the focusing lenses. More on

| Energy (keV) | area ratio peak 4/peak 2 |
|---|---|
| 60 | 18.7 |
| 90 | 18.1 |
| 120 | 24.5 |

**Table 1:** Table showing area ratios between peak 4 and 2 for several different energy tin ions.

that can be found in section 4.4.

To take a look into what can be improved upon for future experiments, it is good to mention that the goal is to eventually be able to compare the different spectra to each other. However to do that, the counts must be normalized. For example, peak 4 is much higher in figure 4.1a than in figure 4.1b, so one could say that the reaction cross section is much larger for $60keV\ Sn^{5+}$ than for $90keV\ Sn^{5+}$. However, the measurement for $60keV\ Sn^{5+}$ could have taken much longer or have a higher current of projectile tin. Therefore, to properly compare the spectra, the current and measurement time must be taken into account. The challenge is then to become able to actively monitor the pulsed beam current, so the different spectra can be compared to each other. Secondly, not much is known on the validity of the ratios between the peak areas, since it is unknown which fraction of all ions created in the reaction actually landed on the MCP. So for that, additional experiments varying the lens settings should be made.

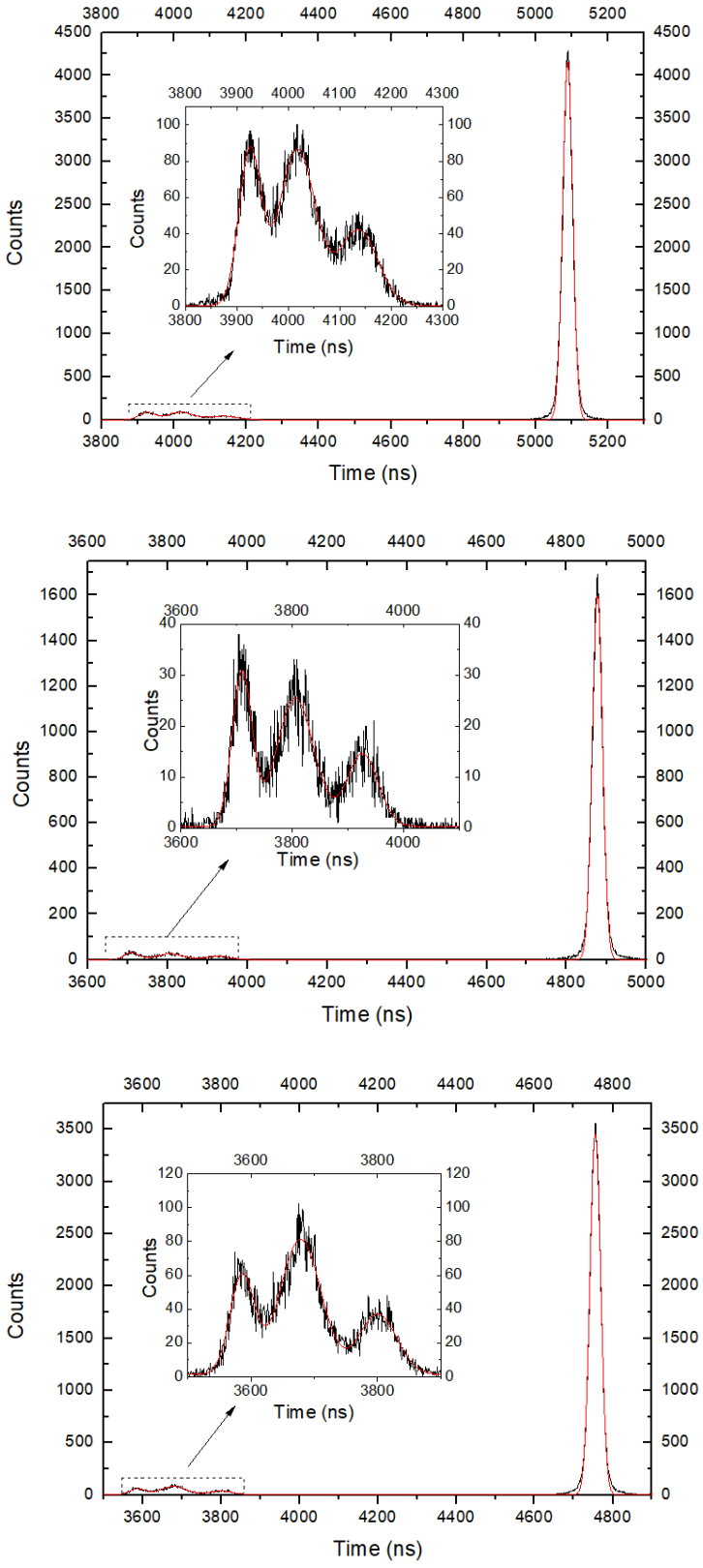


**Figure 4.1:** ToF spectra for 60 $keV$, 90 $keV$ and 120 $keV$ $Sn^{5+}$ions respectively. (Proton) peaks 1, 2 and 3 are enlarged and shown in the same diagram.

## 4.2 Measurements with $OH^+$ as projectile ions

As mentioned in the previous section, it is very important to scan through the isotopes of the desired ion species to make sure the ion current measured is not due to contamination of other species. In this experiment, the 110° magnet was set to a magnetic field ideal for $120keV\ Sn^{7+}$, so a mass-to-charge ratio $\frac{m}{q} = 17.1$. However it later turned out that the tin oven was empty. But still a beam was detected, so we checked to see what other atoms or molecules with $\frac{m}{q} \approx 17.1$ could have produced a solid ion beam. After a short discussion it was concluded that the present ion had to be $OH^+$. The following spectrum was measured:

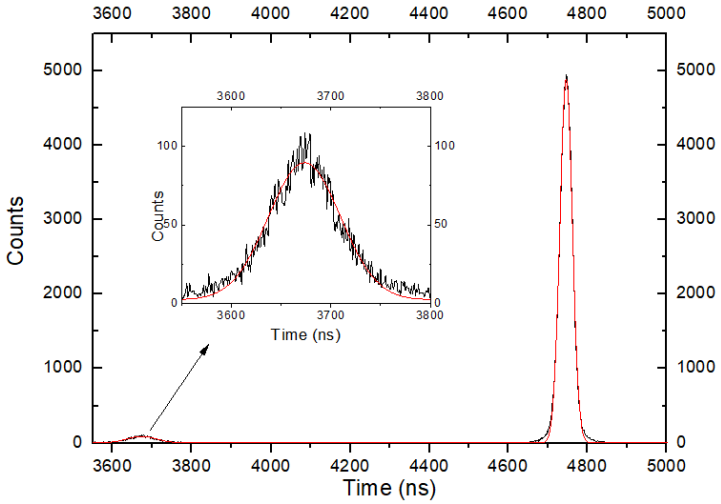


**Figure 4.2:** ToF spectrum for $OH^+$, with the first peak shown enlarged in the same diagram. Notice how there is only 2 peaks instead of 4.

It is very clear from the graph that instead of four peaks, only two can be seen. The question rises which of the four peaks seen in the tin ToF spectra are also seen in this diagram. The best way to find out is to compare the peaks to the 120 $keV\ Sn^{5+}$ peaks, since ions with equal $\frac{m}{q}$ ratio move in the same way inside a vacuum. Using this information, one can see that peak 2 of figure 4.1c has its peak at around 3690 $ns$, just like peak 1 of figure 4.2. Similarly, peak 4 of figure 4.1c has a peak at 4750 $ns$, just as peak 2 of figure 4.2. We can therefore conclude that peak 1 and 2 of the $OH^+$ ToF spectrum correspond to the near zero-energy proton reaction and $H_2^+$ reaction, respectively.

This conclusion coincides with the expectation that in the charge exchange between $OH^+$ and $H_2$, no two electrons can be removed from $H_2$ to generate two fast protons. Additionally, in one-electron capture not enough energy is gained to create a fast proton and hydrogen atom. The reason this happens is the fact that the binding energy of the outermost electron in $OH$ is smaller than the outermost electron in $H_2$. Therefore it would actually cost energy for the electron to move from the hydrogen molecule to the $OH^+$ ion.

The measurements on $OH^+$ were not actually meant to be done in the first place. However they do nicely underscore our understanding of the interactions on $H_2$. So the experiment was a success on its own, and doesn't have to be improved upon or repeated in the future.

## 4.3 Effect of extraction voltage on transmission through diaphragm

In his thesis about molecular dissociation, Hein Otto Folkerts dives deep into the effects of different parameters on the transmission of ions through a diaphragm [5]. The biggest effect of the extraction

voltage on the transmission, is on the relative peak area difference between peak 1 and 3. These are the peaks that originate from protons which have either a net forward or backward starting velocity. One can already intuitively predict how the extraction voltage would affect the peak area ratio between peak 1 and 3, after reading section 2.3. Imagine for example an infinitely high extraction voltage. In that case, all backwards going protons and $H_2^+$ molecules would still be transmitted through the diaphragm, since their acceleration towards the diaphragm would be infinitely high. Because of the fact that the initial velocity direction is random for all reactions, one would expect peak 1 to have the same area as peak 3.

For several extraction voltages between 20V and 100V, the relative peak areas of peak 1 and 3 were measured. The formulas provided in Hein Otto Folkerts' thesis were used to produce theoretical values for the ratio between peak 1 and 3 at the same voltages. The result can be seen in figure 4.3.

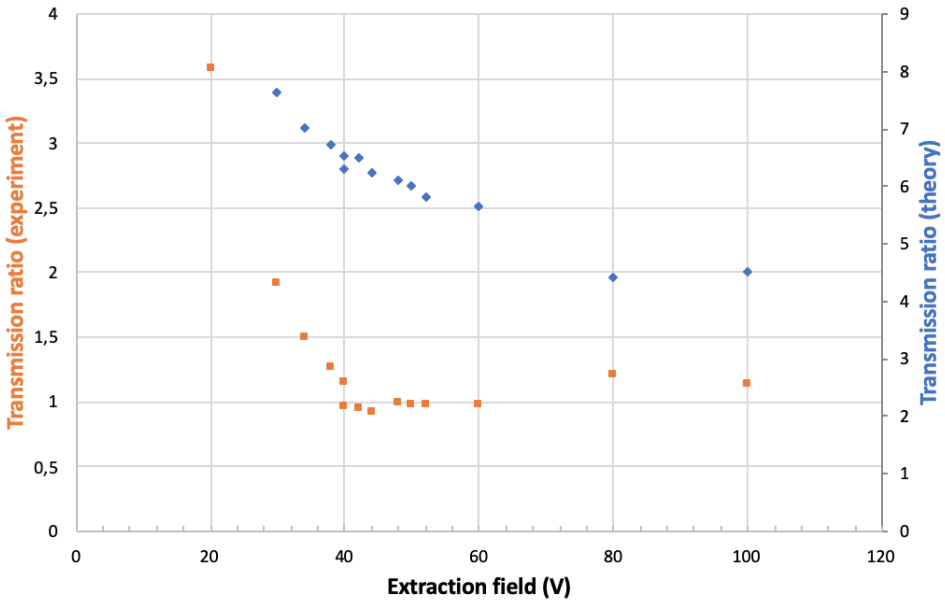


**Figure 4.3:** Diagram showing the transmission ratio between peak 1 and 3 from theory (blue dots) and experiment (orange dots).

In both graphs you can see that the transmission ratio decreases as the extraction field is increased, just as predicted. However it can be clearly seen that the transmission ratio goes toward a value of 1 much quicker in the experiment than was theoretically predicted.

To decrease the discrepancy between the theoretical and experimental values for the transmission fractions, a critical look can be cast upon the transmission model used. The model is inaccurate in two ways. Firstly, the model predicts transmission fractions through or exactly after the diaphragm, while in the setup the reaction products also pass a set of focusing lenses and travel through the ToF tube into the MCP where they are detected. Secondly, the transmissions are determined by the model as if all reactions were to take place in the center of the reaction chamber. Of course, in the setup, the reactions take place within a specific region inside CHEOPS instead of only exactly in the middle. So instead of a simple formula model, a more sophisticated model should be made which takes both the reactions' spacial distribution and the flight time of the ions into account. Such a model can accurately simulate what's happening inside CHEOPS and the ToF tube. This model would then be able to reliably predict transmission ratios as determined in the experiment, so that theoretical and experimental transmission ratios can be compared as accurately as possible

## 4.4 Effect of extraction lens settings on peak areas

To assess whether the focusing lenses play a big role in the reaction product detection, two different lens settings were modeled and tested in an experiment. For the modeling of the needed lens settings, a program called SIMION was used. SIMION is an ion optics simulation program which calculates electric fields for electrodes of defined voltages and determines the ion trajectories in those fields [15].

Two lens settings were modeled. The first would be ideal for protons that start with no initial velocity. The second is ideal for protons that start with a kinetic energy of 8 $eV$, in the direction of the MCP. A picture of how such a simulated ion path looks in SIMION can be found in figure 4.4. In the figure, it seems as if the focusing lenses each consist of an upper an lower plate, which is of course not the same as in the experiment. However SIMION is programmed to calculate the electric field as if the lenses were cylindrical. The radius of the ion beam can be immediately read off the projected ion beam.

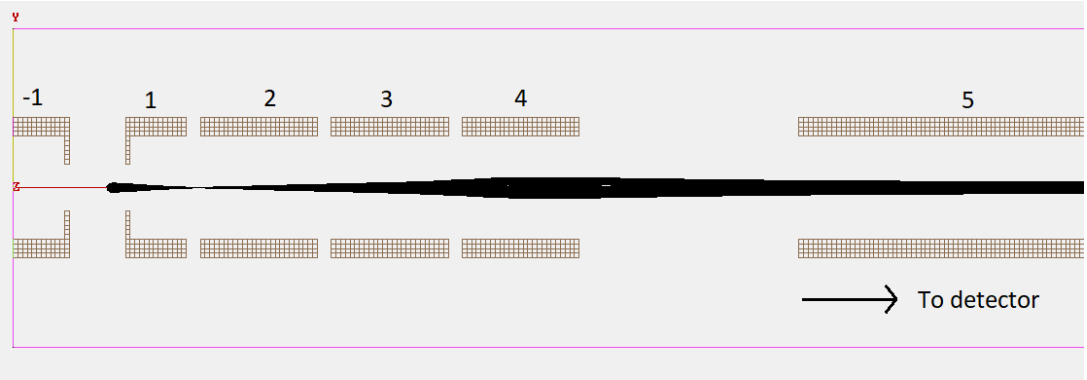


**Figure 4.4:** Picture showing how the extraction plates and focusing lenses are projected in SIMION. The extraction plates are marked -1 and 1. The focusing lenses are marked 2,3 and 4. 5 represents another long cylindrical electrode. The black line represents the simulated ion path.

Using the two modeled lens settings, two measurements were done. The results can be seen in figure 4.5. One can immediately see the difference in the relative peak sizes. With the lens settings optimized for zero-energy protons, clearly peak 2 (representing low-energy protons) is the largest. When using the lens settings optimized for protons with a forward initial kinetic energy, peak 1 (representing protons with a forward initial kinetic energy) is highest. So the model correctly predicts the outcome.

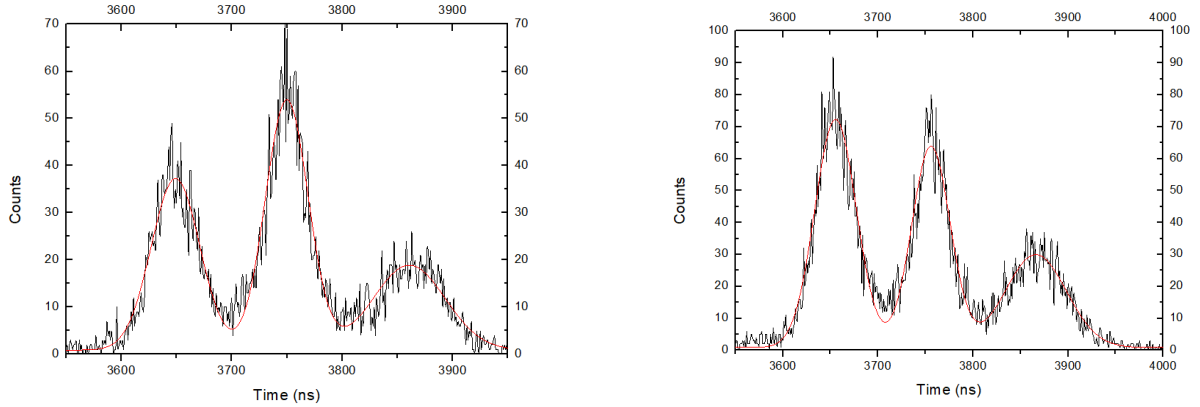


**Figure 4.5:** ToF spectra comparing lens settings optimized for near zero-energy protons (left) and protons with an initial kinetic energy of around 8 $eV$ (right). Shown here are the proton peaks: peak 1, 2 and 3.

This information is quite important. It shows that different lens settings can cause a different outcome.

Of course the question arises, which of the lens settings shows the relative peak heights in a ratio that is closest to what is actually happening in the charge exchange reaction. To answer that, first of all more experiments should be done to get a better sense off how the system responds to the different lens settings by looking at the different ToF spectra.

The model used is something that can potentially be improved upon. Currently, in SIMION you can set the ions' mass, initial energy, the distribution over which they appear and the direction in which they initially move. However, this does not resemble our setup in three ways. First of all, not all ions have the same direction in which they move after the reaction, but they move in all directions. Secondly, the ions don't all have the same initial energy. Lastly, they of course don't all have the same mass (the reaction products are protons as well as $H_{2+}$ molecules). So to make a model that more closely represents the setup, these three factors should be taken into account. The electric fields inside CHEOPS and the ToF tube can still be taken from SIMION, though. If such a model would be made, the lens settings could be altered in such a way that you can make sure that all the reaction products actually hit the MCP. The measurements taken from then on out would then reliably show the reactions and ratios between the reactions that occur inside CHEOPS.

## 4.5 Absolute comparison between $He^+$ and $He^{2+}$ charge exchange reactions

As mentioned in section 4.1, multiple parameters have to be taken into account if you want to accurately compare ToF spectra. This time, the measurement time was noted down and the current was checked regularly. With that information, all counts were divided by the measurement time, the chopping frequency and the particle current. The results can be found in figure 4.6.

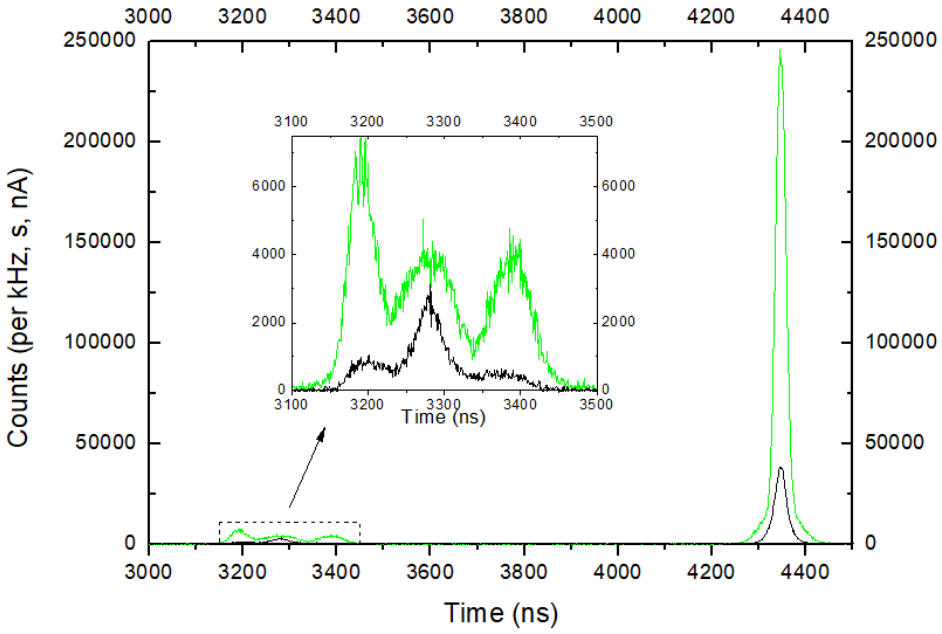


**Figure 4.6:** Comparison of the ToF spectra of $He^+$ (black line) and $He^{2+}$ (green line). Counts are normalized for absolute comparison

A few things immediately stand out. If we first of all separately dissect the spectra, we see that for the $He^+$ spectrum, peak 2 is much higher than peak 1 and 3. This is to be expected, as peak 1 and 3 originate from double electron capture, which is unlikely to happen with a 1+ charge ion. In the $He^{2+}$ spectrum we see that peak 1 and 3 are larger than peak 2, suggesting that double electron capture happens more often, as is to be expected.

If we now compare the spectra to each other, some more interesting findings can be seen. Most importantly, all peaks are much larger for the $He^{2+}$ spectrum than the $He^{+}$ spectrum. This difference can be seen most prominently in peak 4. This suggests that the electron capture cross-section is much higher for $He^{2+}$ than $He^{+}$, which is to be expected. The reason for this is the fact that $He^{2+}$ can capture electrons resonantly while the charge exchange between $He^{+}$ and $H_2$ is dominated by non-resonant capture [9].

There are some remarks concerning this experiment. First of all, the ion beam current was fluctuating greatly. This means that the average current could be quite uncertain, which affects the absolute values of the counts. As mentioned in section 4.1, it would be very useful to find a way to actively monitor the pulsed beam current. Also, this measurement was done on the last day, so there are no other measurements that can support the validity and accuracy of the measurements that were done. Since the experimental setup is quite complex with many fluctuations, multiple experiments should be done to achieve accurate results.

# 5 Conclusion

This thesis builds on previous theses installing and calibrating the experimental setup, and provides a first look into how different ions exchange charge with hydrogen and are affected by several parameters in the setup. The first measurements on tin ions were done, which behave according to theory. Little quantitative research was done, since much of the research was done with the purpose of seeing how the system would respond to changes made in the setup. However, the qualitative research that was done lays a foundation for the step towards quantitative measurements.

The purpose of this thesis is then to sum up the conclusions that can be drawn from all different experiments, and provide advice on how future experiments can improve the setup and experimental results. With correct modeling and adjustments on the focusing lenses and ion paths, results can be obtained that are very close to nature.

## Acknowledgements

The last couple of months have taught me that actual real research is much different and more exciting than the research courses throughout my undergraduate degree. For that, I first have to thank Ronnie Hoekstra for the opportunity to see what doing research is really like. Secondly I would like to thank Subam Rai for his continued help and guidance throughout the experiment. I also owe a great lot of thanks to Roeland Kamp, who on many an occasion helped me better understand the setup and the results obtained, things that would often puzzle me. Lastly I want to thank the members of the QISD group for the, some times very insightful, other times very fun, coffee and lunch breaks throughout my time in the group.

# References


[1] Rachel Courtland. Intel now packs 100 million transistors in each square millimeter. https://spectrum.ieee.org/nanoclast/semiconductors/processors/intel-now-packs-100-million-transistors-in-each-square-millimeter, March 2017.

[2] ASML. An explanation on the technology used at asml. https://www.asml.com/en/technology#lithography.

[3] Heise Magazine. Chipfertigung mit euv-licht und open-source-uefi. https://www.heise.de/select/ct/2018/23/1541827361065226, 2018.

[4] Marten Johannes Deuzeman. *Generation and interactions of energetic tin ions*. PhD thesis, University of Groningen, 2019.

[5] Hein Otto Folkerts. *Molecular dissociation induced by electron transfer to multicharged ions*. PhD thesis, 1996.

[6] A Niehaus. A classical model for multiple-electron capture in slow collisions of highly charged ions with atoms. *Journal of Physics B: Atomic and Molecular Physics*, 19(18):2925, 1986.

[7] Uni Frankfurt. The over-barrier-model. https://www.atom.uni-frankfurt.de/research/40_ion_collisions/10_slow_collisions/20_Over-Barrier-Model/.

[8] Steven Knoop. *Electron Dynamics in Ion-Atom Interactions*. PhD thesis, 2006. $\mathrm{date}_s ubmitted$ : $2006 Rights : UniversityofGroningen$.

[9] Fresia Alvarado Chacon. *Ion induced radiation damage on the molecular level*. PhD thesis, University of Groningen, 2007.

[10] Erik Berends. *Energetic ions traversing hydrogen gas: fragmentation of hydrogen molecules*. BSc Thesis, University of Groningen, 2019.

[11] Wikipedia contributors. Einzel lens — Wikipedia, the free encyclopedia. https://en.wikipedia.org/w/index.php?title=Einzel_lens&oldid=874277407, 2018.

[12] Santiago Bernal. Linear magnetic lenses and deflectors. In *A Practical Introduction to Beam Physics and Particle Accelerators*, 2053-2571, pages 2–1 to 2–15. Morgan Claypool Publishers, 2016.

[13] Kashif Chaudhary, Syed Zuhaib Haider Rizvi, and Jalil Ali. Laser-induced plasma and its applications. In Tetsu Mieno, editor, *Plasma Science and Technology*, chapter 11. IntechOpen, Rijeka, 2016.

[14] Del Mar Photonics. Microchannel plates and mcp detectors and imaging systems. http://www.dmphotonics.com/MCP_MCPImageIntensifiers/mcp_references.htm.

[15] David A. Dahl. simion for the personal computer in reflection. *International Journal of Mass Spectrometry*, 200(1-3):3–25, Dec 2000.